

Effect of Si doping on the electronic properties of BN monolayer†

Cite this: *Nanoscale*, 2014, 6, 5526

Sanjeev K. Gupta,^a Haiying He,^b Douglas Banyai,^a Mingsu Si,^{‡a} Ravindra Pandey^{*a} and Shashi P. Karna^c

The effect of Si doping on the stability, electronic structure, and electron transport properties of boron nitride (BN) monolayer has been investigated by density functional theory method. Unique features in the electron transport characteristics consisting of a significant enhancement of current at the Si site, diode-like asymmetric current–voltage response, and negative differential resistance are noted for the doped BN monolayer. These features are found to result from new “tunnel” channels induced by the substitutional Si atom near Fermi level in the band gap. The calculated position-projected tunneling currents providing scanning tunneling micrograph clearly discern the site-dependence of the Si atom and can be used to distinguish substitutional sites of atomic dopants in the monolayer.

Received 10th January 2014
Accepted 23rd February 2014

DOI: 10.1039/c4nr00159a

www.rsc.org/nanoscale

I. Introduction

Thin films of BN have been a subject of extensive studies over the past two decades.^{1–12} Unlike a semi-metallic graphene, BN consisting of a few layers has a finite band gap,¹⁰ which allows it to be used as a dielectric material in electronic devices at nanoscale. In fact, several recent experiments have demonstrated the use of two-dimensional BN as a dielectric material in graphene, graphite, and Au electrode-based devices.⁷ In recent years, the focus of theoretical and experimental studies is shifted towards determining the role of dopants in the BN monolayer.^{13–19} For example, magnetism in a BN sheet induced by nonmagnetic impurities is predicted.¹⁴ The spin-polarized density of states of dopants, such as Be, C, O, Al, and Si atoms clearly find them to be at least paramagnetic in BN.¹⁴ A theoretical study investigated the C doped BN monolayer addressing the effects of many parameters like the choice of chemical potential and atom displacement cross sections for the substitutional process in the lattice.¹⁹ Since Si plays a dominant role in electronics, its role in the BN nanostructures including thin films and nanotubes has been extensively investigated.^{15,20–24} The experimental studies characterizing Si-doped multi-walled boron nitride nanotubes (BNNTs) have shown the formation of

Si–B and Si–N bonds in the lattice.^{20,21} Si doping has also induced spontaneous magnetization in the (5,5) BNNT.²⁰ In Si-doped graphene, on the other hand, a new kind of chemical bonding induced by the participation of Si electrons is revealed despite its isovalency with C in the lattice.²⁵

Since Si has a different number of valence electrons than the constituent atoms of the BN monolayer, one can expect significant modification of electron transport properties of the semiconducting monolayer in a somewhat similar way as doping of bulk Si by B or N atoms. This is what we propose to investigate in this paper using density functional theory within generalized gradient approximation. Initially, we calculate stability and electronic structure of Si-doped monolayer. Later, we calculate its electron transport properties in a model setup where the monolayer is supported on the Au substrate. The computational details are given in Section II. In Section III, we discuss the results, and a brief summary is given in Section IV.

II. Computational method

The spin-polarized electronic structure calculations were carried out in the framework of the density functional theory (DFT). The generalized gradient approximation (GGA) of Perdew, Burke and Ernzerhof²⁶ was used to include the exchange and correlation functionals. The projector augmented wave (PAW) method as implemented in the Vienna *ab initio* simulation package (VASP) code²⁷ was used for calculations.

The supercell approach with periodic boundary conditions was applied to describe the pristine and Si-doped BN monolayers. For the pristine BN monolayer, a (1 × 1) supercell was used, while a (5 × 5) supercell was used for the Si-doped monolayer to ensure minimal interaction of Si with its neighboring images. A 10 Å vacuum was adopted along the direction

^aDepartment of Physics, Michigan Technological University, Houghton, Michigan 49931, USA. E-mail: pandey@mtu.edu

^bDepartment of Physics and Astronomy, Valparaiso University, Valparaiso, IN 46383, USA

^cUS Army Research Laboratory, Weapons and Materials Research Directorate, ATTN: RDRL-WM, Aberdeen Proving Ground, MD 21005-5069, USA

† Electronic supplementary information (ESI) available. See DOI: 10.1039/c4nr00159a

‡ Permanent address: Key Laboratory for Magnetism and Magnetic Materials of MOE, Lanzhou University, Lanzhou 730000, People's Republic of China.

perpendicular to the plane of the sheet. The structures were fully optimized using the energy/force relaxation approach. The cutoff energy for the plane wave basis was 500 eV. The convergence criterion of optimization was $0.03 \text{ eV } \text{\AA}^{-1}$ for the force on each ion and 10^{-5} eV for the total energy convergence. The Brillouin zone is sampled using a $5 \times 5 \times 1$ Monkhorst-Pack grid for integration in the reciprocal space for the Si-doped monolayers. Note that the use of $9 \times 9 \times 1$ grid for integration changed the value of total energy of Si-doped BN monolayer for 3-fold site only by 0.1 eV.

The transverse electron transport properties of the pristine and Si-doped monolayers supported on the Au substrate were calculated using a model setup as used in Scanning Tunneling Microscopy (STM). The spin-polarized electron tunneling current through the monolayer between the Au substrate and a metal tip was calculated based on the Bardeen, Tersoff, and Hamann (BTH) formalism.^{28–30} The supercell in transport calculations is chosen in such a way that the lattice of BN is commensurate with that of Au (111) surface (see the top view of the lattice match in the ESI, Fig. S1†). A (4×6) supercell consisting of 24 B and 24 N atoms is taken for the pristine BN monolayer. For Si-doped BN monolayer, the same dimensions along the x and y directions are kept with one or two host atoms being substituted by a Si atom. A four-layer slab with 18 atoms per layer is used to simulate the bare Au substrate. The distance between the BN monolayer and the Au substrate is taken to be 3.0 \AA as optimized in our earlier studies.^{31,32}

The cap configuration of the metal tip is modeled by a 13-atom Au icosahedral cluster. The density of states for the tip is broadened using a Gaussian broadening scheme with a width of 0.2 eV to account for the semi-infinite nature of the tip. The tip is considered to be separated from the in-plane BN monolayer by a vacuum barrier width of 5 \AA , mimicking a non-bonded tip configuration for the STM measurements.^{29,30} Due to the off-plane distortion occurring for some of the Si-doped cases, the actual distance between the atom of the 2D monolayer and the tip may be slightly less than 5 \AA . The work function of the BN monolayer, defined as the energy difference between the electrostatic potential at the vacuum-level and the Fermi energy of its surface, is calculated to be 4.8 eV (ESI, Fig. S2†). The work function of the tip is taken to be 6.67 eV, the experimental value of the ionization potential of the Au_{13} cluster.³³

III. Results and discussion

Equilibrium structure and stability

Two kinds of substitution sites are considered for Si in the BN sheet: (i) Si atom substituting a single B (Si_B) or N atom (Si_N), where the Si atom has a 3-fold coordination with three neighboring N/B atoms; (ii) Si substituting for a divacancy site created by the removal of a B–N pair (Si_BN). In this configuration the Si atom has a 4-fold coordination with neighboring atoms. In the equilibrium structure, the pristine BN monolayer is calculated to have a planar configuration with the bond length of 1.45 \AA , in good agreement with the corresponding experimental value of 1.44 \AA .⁶ Our calculated value is also in agreement with the

previously reported values of 1.459 \AA obtained using vdW-DFT³¹ and 1.45 \AA obtained using GGA-DFT¹⁶ calculations.

In the equilibrium configurations for Si_B and Si_N , there is out-of-plane geometry around Si; the dopant protrudes 1.2 \AA and 1.7 \AA from the monolayer plane for Si_B and Si_N , respectively (see the side view—Fig. S3†). The in-plane symmetry of the monolayer is broken and Si forms a tetrahedral structure with three neighboring atoms taking a sp^3 -like hybridization. For the case of Si_B , the dopant is connected to three nearest N atoms with equal Si–N bond length of $\sim 1.71 \text{ \AA}$. The next nearest neighbor distance is $\sim 2.71 \text{ \AA}$. On the other hand, Si_N is connected to three nearest B atoms with equal Si–B bond length of $\sim 1.96 \text{ \AA}$. The next nearest neighbor distance for Si_N is $\sim 2.94 \text{ \AA}$ for Si_N . The charge density contour maps (Fig. 1) for Si_B and Si_N show that the perturbation from the dopant is symmetrically superimposed on the atoms around it. Thus, Si takes a symmetric position and forms the equidistance bonds with the three nearest neighbors in the lattice. This is not the case with Si_BN where the structure around the dopant site is completely different. In this case (Fig. 1(c)), a relatively large overlap of Si with two nearest N atoms is seen. The 4-fold coordinated Si_BN prefers an in-plane configuration in which Si takes a sp^2 -like hybridization and forms four in-plane bonds with neighboring B and N atoms with greater overlap with N atoms than with the B atoms. The energies of the in-plane configurations are 2.73 eV and 2.56 eV higher than energies for the ground state configurations for Si_B and Si_N , respectively. The Si–N bond length (1.79 \AA) for the 4-fold Si_BN is slightly larger than that for the 3-fold Si_B (1.71 \AA), whereas the Si–B bond length (2.12 \AA) is significantly larger than that in the 3-fold Si_N (1.96 \AA).

Calculations of the formation energies [see ESI† for details, ^{13,34}] suggest that the Si substitution at the N site in the monolayer will be an energetically demanding process, though the formation of Si_B is always preferred over Si_N and Si_BN under either N-rich or B-rich conditions. Especially under the N-rich condition, the doping of Si at the B site (Si_B) is thermodynamically quite favorable. A comparison of our results with the results on the C-doped BN monolayer¹⁹ shows a similar variation in the formation energy of C_B and C_N . Note that doping of Si

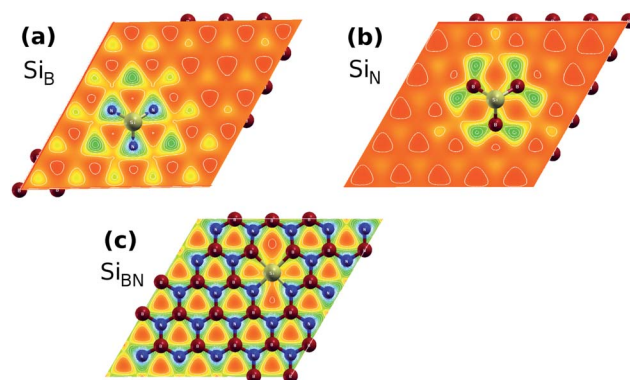


Fig. 1 The charge density contours ($1/8^{\text{th}}$ ($0.0003 \text{ e } \text{\AA}^{-3}$) of the maximum value) of Si doped BN monolayers: (a) Si_B , (b) Si_N , and (c) Si_BN .

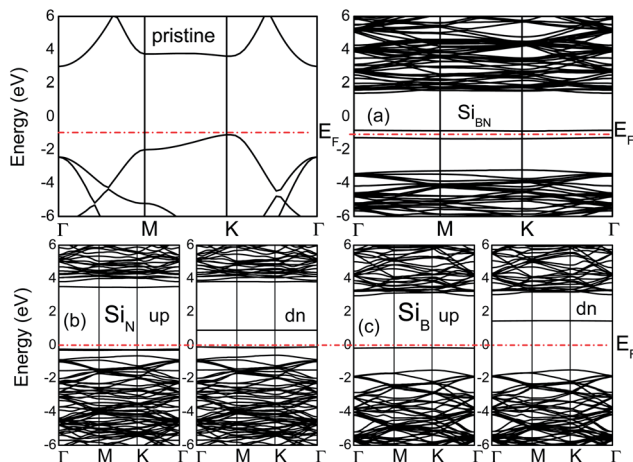


Fig. 2 The calculated band structures of pristine BN and Si doped monolayers: (a) Si_B , (b) Si_N , 'up' and 'dn' refer to the spin-up and spin-down components of the band structure. The dotted line represents Fermi energy (E_F) of the system.

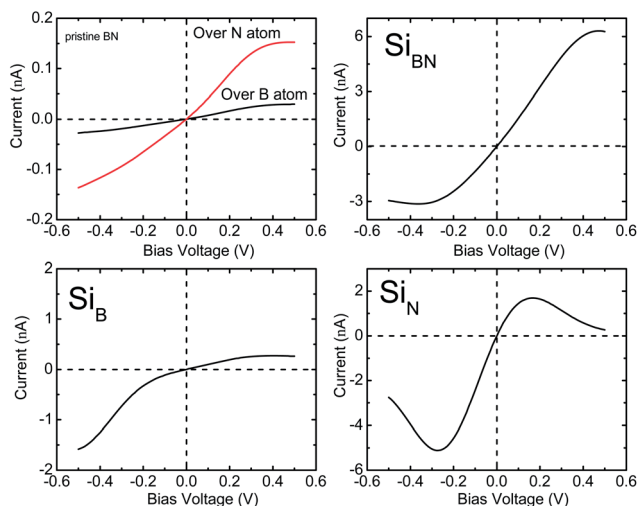


Fig. 3 The current–voltage characteristics of (a) pristine (b) Si_B (c) Si_B , and (d) Si_N -doped BN monolayers.

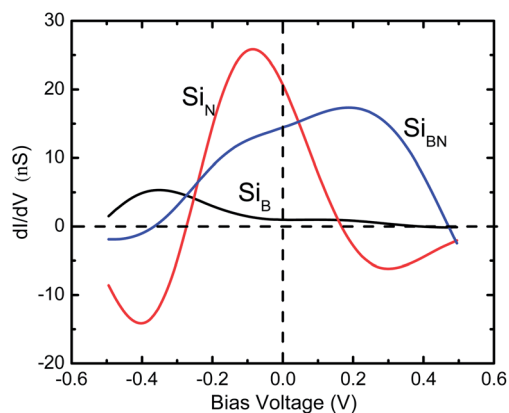


Fig. 4 The calculated differential conductance curve of the Si-doped monolayers deposited on the Au (111) substrate.

in BN nanotubes was theoretically investigated.²² Subsequently, synthesis of Si-doped BN nanotubes by thermal chemical vapor deposition, and catalyst-assisted pyrolysis of polymeric precursor have been reported.^{23,24} In addition, Si-doped BN thin films were synthesized by *in situ* co-sputtering during ion beam assisted deposition.¹⁵ Synthesis of Si-doped BN monolayer is therefore expected to be feasible.

Electronic properties

Fig. 2 shows the calculated band structures of pristine and Si-doped BN monolayers. The top of valence band is primarily composed of N-p states, while the bottom of the conduction band is mainly consisted of B-p states. A direct gap of 4.4 eV is calculated near the k -point for the pristine BN. This agrees well with the previously reported theoretical values of 4.6 eV.³¹ However, the calculated value is smaller by ~ 1.3 eV compared to the experimental value for the bulk hexagonal (h)-BN.³⁵

The spin resolved band structure of the Si doped monolayer retains most of the features of the pristine monolayer. Appearance of the so-called mid-gap states suggests that the change in the electronic structure induced by doping is likely to be localized in the vicinity of Si. This is confirmed by analysis of the density of states (DOS) revealing that the mid-gap state is primarily from the Si-s and Si-p states (Fig. S5[†]) in agreement with the previously reported study.¹⁴

The mid-gap states for Si_B located at 1.3 eV and 2.9 eV above the valence band maximum (VBM) for the spin-up and spin-down electrons, respectively. The gap state is a donor state, which splits from the conduction band and moves down in energy as the dopant relaxes from an in-plane configuration to an out-of-plane configuration (see ESI, Fig. S6[†]). The α -orbital becomes occupied, while the β -orbital remains unoccupied, leading to spontaneously induced magnetization in the monolayer. The net magnetic moment per unit cell is calculated to be $1 \mu_B$. In this work, the spin density plot reveals that the spin is mainly distributed on Si (70%) with only a small part (30%) on the nearest N atoms (see ESI, Fig. S7[†]). Our results are consistent with the results reported for the C_B doped BN monolayer,¹⁹ transition metal doped BN monolayer^{17,18} and Si-doped BNNT.²⁰

There exist four distinct states within the band gap for Si_N which is nearly dispersion-less. Three of them are nearly degenerate and located about 0.4 eV above VBM for the spin-up case, while one of them splits from the rest lying 1.5 eV above VBM for the spin-down case (Fig. 2). Analysis of DOS (see ESI, Fig. S5[†]) suggests that the occupied mid-gap states to be composed of Si, N and B orbitals. On the other hand, Si and B orbitals form an unoccupied band located near the conduction band minimum (CBM). Our results on Si-doped BN sheet are different from the reported results on Si-doped BNNT where only two mid-gap states appear for Si_N .²⁰ The difference can be attributed to the curvature effect which removes the 3-fold degeneracy of the Si dopant in the BN monolayer.

Two gap states separated by about 0.4 eV are seen in the band gap (Fig. 2) for Si_B . The lower one is occupied while the upper one is not. The lower-energy gap state is a hybridization of Si-p, Si-d and B-p states, while the higher-energy gap state is

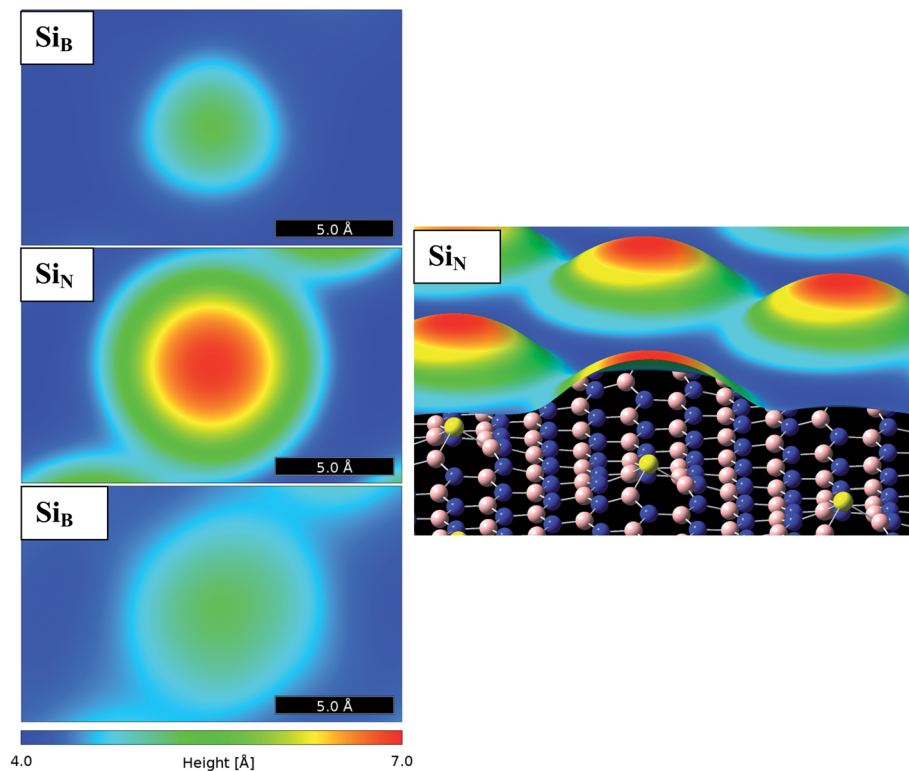


Fig. 5 The STM images at constant current (1 nA, 100 mV) for Si doped monolayers: (a) Si_B, (b) Si_N, and (c) Si_{BN}; and (d) a cutaway perspective image of the constant current surface for Si_N.

primarily from Si-p (see ESI, Fig. S5 and S6[†]). No spontaneous magnetization was found, and the energy of a triplet state ($2 \mu_B$) is about 0.5 eV higher than the non-magnetic state for Si_{BN}.

Electron transport properties

The electron transport properties are intimately related to the electronic structure of a material. Therefore, any modification of the electronic structure of the pristine BN monolayer is expected to significantly influence its electron transport properties. In the present study, we modeled conventional STM setup to calculate the tunneling current through the monolayer deposited on the Au (111) substrate (Fig. S8[†]). The cap configuration of the STM tip is represented by the Au₁₃ cluster. The calculated tunneling currents associated with pristine and doped BN monolayers are plotted in Fig. 3 over the range of -0.5 V to 0.5 V. We define the bias to be positive when the gold substrate and the BN monolayer are connected to a positive potential and electrons tunnel from the tip to the monolayer. It is to be noted that the tunneling current depends exponentially on the separation of the tip to sample. Therefore, the choice of tip-sample separation will determine the magnitude of the tunneling current, but should not affect the predicted trend described below.^{28–30} For example, increase in the tip-sample separation from 5 \AA to 10 \AA decreases the conductance by several orders of magnitude in our case (see ESI, Fig. S9[†]).

For the pristine monolayer, the threshold voltage is about 5 mV and the tunneling current over either B or N atom shows an approximately linear relationship with voltage. Also, the

current through N is much higher (reaching $\sim 0.1 \mu\text{A}$ at 0.5 V) than that through B (reaching $\sim 0.02 \mu\text{A}$ at 0.5 V). It is consistent with the fact that the N states dominate near Fermi for the pristine monolayer. Recent experiments⁷ on atomically thin, defect-free h-BN layers sandwiched between two similar electrodes of graphene or gold have demonstrated tunneling behavior of the architecture with approximately linear I - V characteristics at low bias.

The Si-doped monolayer exhibits remarkable electron transport properties. To start, for Si-doped monolayers, the tunneling current over the dopant Si is higher than that over the constituent (B/N) host atoms. Second, the transverse tunnel current sampled at the Si atom at various substitutional sites of the BN monolayer, exhibits a highly asymmetric behavior with respect to the polarity of the external bias (Fig. 3). For Si_B and Si_N, the magnitude of tunneling current under the negative bias (with electrons tunneling from the monolayer to the tip) is higher than that under the positive bias (with electrons tunneling from the tip to the monolayer), while the case is the reverse for Si_{BN}. It is interesting to point out that one can distinguish different substitutional sites by evaluating their images under positive and negative biases. For example, Si_B will give the largest variation in its brightness switching from positive to negative bias ($I_-/I_+ \sim 7$), while Si_N ($I_-/I_+ \sim 4$) and Si_{BN} ($I_-/I_+ \sim 1/3$) will have less variation in their positive and negative responses.

Since the tunneling current is an integration of the convolution of DOSs of the tip and the sample, it is apparent that a

large tunneling current over the Si atom is due to the induced gap states owing to the dopant in the monolayer. These gap states are lined up near the Fermi level and are the major tunneling “channels” under an applied bias. Furthermore, since these gap states are distributed asymmetrically in the positive and negative energies around the Fermi level, the tunneling currents associated with the dopant Si are also shown to be asymmetric under positive and negative biases. Note that the interaction of the BN monolayer with the Au substrate allows the gap state to be broadened as compared to those without the substrate, Au. The Bader charge analysis reveals a transfer of about 0.1 e, 0.3 e, and 0.4 e charge from the Si_N, Si_B and Si_{BN} of BN monolayers to Au, respectively. Specifically, the transfer of charge from Si_{BN} to Au shifts down the Fermi level, crossing the DOS peak originating from the Si states. This leads to a relatively higher tunneling current at Si_{BN} compared to that at Si_B and Si_N. The induced Si-related mid-gap states, which are spin-polarized due to aliovalent nature of the dopant, lead to the spin-polarized tunneling currents for Si_B and Si_N.

The distinct features of the mid-gap states in the doped monolayers also lead to the resonant tunneling phenomena, where the negative differential resistance (NDR) effect is predicted, and is reflected in the differential conductance (Fig. 4). The correspondence between the NDR peak and the mid-gap state thus provides a useful tool for tailoring the transport properties in semiconducting materials at nanoscale. We expect this feature of the transport property of the Si-doped BN monolayer to be useful in the low-power memory applications and logic circuit devices.

The simulated STM images generated from the position-projected tunneling currents are shown in Fig. 5. The location of the Si atoms is clearly visible in all cases, and each case is discernible from the other. For the Si_B configuration, the STM image height can be primarily attributed to the physical protrusion of the Si atom. In this configuration, the 3-fold symmetry is subtly discernible, again attributable to the protrusion of the nearest neighbors. For the Si_N configuration, the ~3 Å image height is approximately twice the out-of-plane distance of Si, indicating the change in the electronic structure is much more significant than that for the Si_B case.

IV. Conclusions

Ultrathin films of BN have emerged as a stable, high-purity, highly desirable nano-scale dielectric material. The present study explores and identifies the possibility of developing Si-doped BN monolayers for electronic devices at nanoscale. The results indicate that Si substitution for B (forming Si–N bonds) is favored over Si substitution for N (forming Si–B bonds). The Si–N bond for Si_B is rather strong with a bond length of 1.71 Å, close to the corresponding Si–N single bond length. The unpaired electron in the Si_B and Si_N substitutions induces a magnetic moment (~1 μ_B) in the system. The spin is primarily located on the 3p orbital of the Si atom. The 4-fold Si_{BN} configuration, however, has no magnetism, and Si takes a sp²d type of hybridization in its in-plane monolayer configuration.

Si-induced gap states in the band energy of the BN monolayer have profound effect on the electronic structure and electron transport properties. The transverse tunnel current through Si-doped monolayer has significantly higher magnitude than through pristine monolayer. The current–voltage curves sampled at the substitutional Si sites exhibit remarkable asymmetric response due to the polarity of the bias voltage. The doped monolayer also exhibits a negative differential resistance behavior in its *I–V* characteristics, which is very prominent at Si_N site. The calculated position-projected tunneling currents providing scanning tunneling microscopic images clearly discern the site-dependence of the Si atom. New applications of Si-doped BN monolayers in nanoscale devices may be expected due to the spin-polarized electronic and magnetic properties they possess.

Acknowledgements

S.K.G. acknowledges award of the Fulbright-Nehru Postdoctoral Research Fellowship by United States-India Educational Foundation (USIEF) and Grant no. 1638/FNPDR/2012. Helpful discussions with S. Gowtham are also acknowledged. RAMA and Superior, high performance computing clusters at Michigan Technological University, were used in obtaining results presented in this paper.

References

- 1 A. R. Phani, Thin films of boron nitride grown by CVD, *Bull. Mater. Sci.*, 1994, **17**, 219; A. Phani, S. Roy and V. J. Rao, Growth of boron nitride thin films by metal-organic chemical vapour deposition, *Thin Solid Films*, 1995, **258**, 21.
- 2 J.-L. Huang, C.-H. Pan and D.-F. Lii, Investigation of the BN films prepared by low pressure chemical vapor deposition, *Surf. Coat. Technol.*, 1999, **122**, 166.
- 3 A. H. M. A. Wasey, S. Chakrabarty, G. P. Das and C. Majumder, h-BN Monolayer on the Ni(111) Surface: A Potential Catalyst for Oxidation, *Phys. Rev. Lett.*, 1995, **75**, 3918.
- 4 G. B. Grad, P. Blaha, K. Schwarz, W. Auwärter and T. Greber, Density functional theory investigation of the geometric and spintronic structure of h-BN/Ni(111) in view of photoemission and STM experiments, *Phys. Rev. B: Condens. Matter*, 2003, **68**, 085404.
- 5 G.-H. Lee, Y.-J. Yu, C. Lee, C. Dean, K. L. Shepard, P. Kim and J. Hone, Electron tunneling through atomically flat and ultrathin hexagonal boron nitride, *Appl. Phys. Lett.*, 2011, **99**, 243114.
- 6 F. Orlando, R. Larciprete, P. Lacovig, I. Boscarato, A. Baraldi and S. Lizzit, Epitaxial Growth of Hexagonal Boron Nitride on Ir(111), *J. Phys. Chem. C*, 2012, **116**, 157.
- 7 L. Britnell, R. V. Gorbachev, R. Jalil, B. D. Belle, F. Schedin, M. I. Katsnelson, L. Eaves, S. V. Morozov, A. S. Mayorov, N. M. R. Peres, A. H. C. Neto, J. Leist, A. K. Geim, L. A. Ponomarenko and K. S. Novoselov, Electron tunneling through ultrathin boron nitride crystalline barriers, *Nano Lett.*, 2012, **12**, 1707.

- 8 G. Gao, W. Gao, E. Cannuccia, J. Taha-Tijerina, L. Balicas, A. Mathkar, T. N. Narayanan, Z. Liu, B. K. Gupta, J. Peng, Y. Yin, A. Rubio and P. M. Ajayan, Artificially Stacked Atomic Layers: Toward New van der Waals Solids, *Nano Lett.*, 2012, **12**, 3518.
- 9 M. S. Bresnehan, M. J. Hollander, M. Wetherington, M. LaBella, K. A. Trumbull, R. Cavalero, D. W. Snyder and J. A. Robinson, Integration of Hexagonal Boron Nitride with Quasi-freestanding Epitaxial Graphene: Toward Wafer-Scale, High-Performance Devices, *ACS Nano*, 2012, **6**, 5234.
- 10 L. Song, Z. Liu, A. L. M. Reddy, N. T. Narayanan, J. Taha-Tijerina, J. Peng, G. Gao, J. Lou, R. Vajtai and P. M. Ajayan, Binary and Ternary Atomic Layers Built from Carbon, Boron, and Nitrogen, *Adv. Mater.*, 2012, **24**, 4878.
- 11 A. Nagashima, N. Tejima, Y. Gamou, T. Kawai and C. Oshirna, Electronic Structure of Monolayer Hexagonal Boron Nitride Physisorbed on Metal Surfaces, *ACS Appl. Mater. Interfaces*, 2013, **5**, 10404.
- 12 A. Gibb, N. Alem and A. Zettl, Low pressure chemical vapor deposition synthesis of hexagonal boron nitride on polycrystalline metal foils, *Phys. Status Solidi B*, 2013, **250**, 2727.
- 13 S. Azevedo, J. R. Kaschny, C. M. C. de Castilho and F. de Brito Mota, Electronic structure of defects in a boron nitride monolayer, *Eur. Phys. J. B*, 2009, **67**, 507.
- 14 R.-F. Liu and C. Cheng, *Ab initio* studies of possible magnetism in a sheet by nonmagnetic impurities and vacancies, *Phys. Rev. B: Condens. Matter Mater. Phys.*, 2007, **76**, 014405.
- 15 J. Ying, X. W. Zhang, Z. G. Yin, H. R. Tan, S. G. Zhang and Y. M. Fan, Electrical transport properties of the Si-doped cubic boron nitride thin films prepared by *in situ* cosputtering, *J. Appl. Phys.*, 2011, **109**, 023716.
- 16 S. Noorizadeh and E. Shakerzadeh, Formaldehyde adsorption on pristine, Al-doped and mono-vacancy defected boron nitride nanosheets: A first principles study, *Comput. Mater. Sci.*, 2012, **56**, 122.
- 17 B. Huang, H. Xiang, J. Yu and S.-H. Wei, Effective control of the charge and magnetic states of transition-metal atoms on single-layer boron nitride, *Phys. Rev. Lett.*, 2012, **108**, 206802.
- 18 J. Li, M. L. Hu, Z. Yu, J. X. Zhong and L. Z. Sun, Structural, electronic and magnetic properties of single transition-metal adsorbed BN sheet: A density functional study, *Chem. Phys. Lett.*, 2012, **532**, 40.
- 19 N. Berseneva, A. Gulans, A. V. Krashennikov and R. M. Nieminen, Electronic structure of boron nitride sheets doped with carbon from first-principles calculations, *Phys. Rev. B: Condens. Matter Mater. Phys.*, 2013, **87**, 035404.
- 20 M. S. Si and D. S. Xue, First-principles study of silicon-doped (5,5) BN nanotubes, *Europhys. Lett.*, 2006, **76**, 664.
- 21 Y. J. Cho, C. H. Kim, H. S. Kim, J. Park, H. C. Choi, H.-J. Shin, G. Gao and H. S. Kang, Electronic structure of Si-doped BN nanotubes using X-ray photoelectron spectroscopy and first-principles calculation, *Chem. Mater.*, 2009, **21**, 136.
- 22 S. Guerini, T. Kar and P. Piquini, Theoretical study of Si impurities in BN nanotubes, *Eur. Phys. J. B*, 2004, **38**, 515.
- 23 S. Xu, Y. Fan, J. Luo, L. Zhang, W. Wang, B. Yao and L. An, Phonon characteristics and photoluminescence of bamboo structured silicon-doped boron nitride multiwall nanotubes, *Appl. Phys. Lett.*, 2007, **90**, 013115.
- 24 S. F. Xu and D. Xu, The structure and light emitting of silicon-doped boron nitride nanotubes, *Adv. Mater. Res.*, 2012, **616**, 1898.
- 25 W. Zhou, M. D. Kapetanakis, M. P. Prange, S. T. Pantelides, S. J. Pennycook and J.-C. Idrobo, Direct determination of the chemical bonding of individual impurities in graphene, *Phys. Rev. Lett.*, 2012, **109**, 206803.
- 26 J. P. Perdew, K. Burke and M. Ernzerhof, Generalized gradient approximation made simple, *Phys. Rev. Lett.*, 1996, **77**, 3865.
- 27 G. Kresse and J. Furthmuller, Efficient iterative schemes for *ab initio* total-energy calculations using a plane-wave basis set, *Phys. Rev. B: Condens. Matter*, 1996, **54**, 11169.
- 28 J. Tersoff and D. R. Hamann, Theory and application for the scanning tunneling microscope, *Phys. Rev. Lett.*, 1983, **50**, 1998.
- 29 H. He, R. Pandey, R. Pati and S. P. Karna, Spin-polarized electron transport of a self-assembled organic monolayer on a Ni(111) substrate: An organic spin switch, *Phys. Rev. B: Condens. Matter Mater. Phys.*, 2006, **73**, 195311.
- 30 S. K. Gupta, H. He, D. Banyai, A. K. Kandalam and R. Pandey, Electron Tunneling Characteristics Of A Cubic Quantum Dot, (PbS)₃₂, *J. Chem. Phys.*, 2013, **139**, 244307.
- 31 X. Zhong, R. G. Amorim, R. H. Scheicher, R. Pandey and S. P. Karna, Electronic structure and quantum transport properties of trilayers formed from graphene and boron nitride, *Nanoscale*, 2012, **4**, 5490.
- 32 R. G. Amorim, X. Zhong, S. Mukhopadhyay, R. Pandey, A. R. Rocha and S. P. Karna, Strain- and electric field-induced band gap modulation in nitride nanomembranes, *J. Phys.: Condens. Matter*, 2013, **25**, 195801.
- 33 M. Okumura, Y. Kitagawa, M. Haruta and K. Yamaguchi, DFT studies of interaction between O₂ and Au clusters. The role of anionic surface Au atoms on Au clusters for catalyzed oxygenation, *Chem. Phys. Lett.*, 2001, **346**, 163.
- 34 V. A. Gubanov, Z. W. Lu, B. M. Klein and C. Y. Fong, Electronic structure of defects and impurities in III-V nitrides: Vacancies in cubic boron nitride, *Phys. Rev. B: Condens. Matter*, 1996, **53**, 4377.
- 35 K. Watanabe, T. Taniguchi and H. Kanda, Direct-bandgap properties and evidence for ultraviolet lasing of hexagonal boron nitride single crystal, *Nat. Mater.*, 2004, **3**, 404.